Supplemental Material for: Scanning tunneling microscope-induced excitonic luminescence of a two-dimensional semiconductor

Delphine Pommier,[1] Rémi Bretel,[1] Luis E. Parra López,[2] Florentin Fabre,[2] Andrew Mayne,[1] Elizabeth Boer-Duchemin,[1] Gérald Dujardin,[1] Guillaume Schull,[2] Stéphane Berciaud,[2] and Eric Le Moal[1,*]

[1] *Institut des Sciences Moléculaires d'Orsay (ISMO), CNRS, Univ Paris Sud, Université Paris-Saclay, F-91405 Orsay, France*

[2] *Institut de Physique et Chimie des Matériaux de Strasbourg, Université de Strasbourg, CNRS, IPCMS, UMR 7504, F-67000 Strasbourg, France*

(Dated: June 12, 2019)

In this Supplemental Material, additional STM-induced luminescence spectra are shown. The data analysis, the experimental methods and the excitation mechanisms are discussed in more detail.

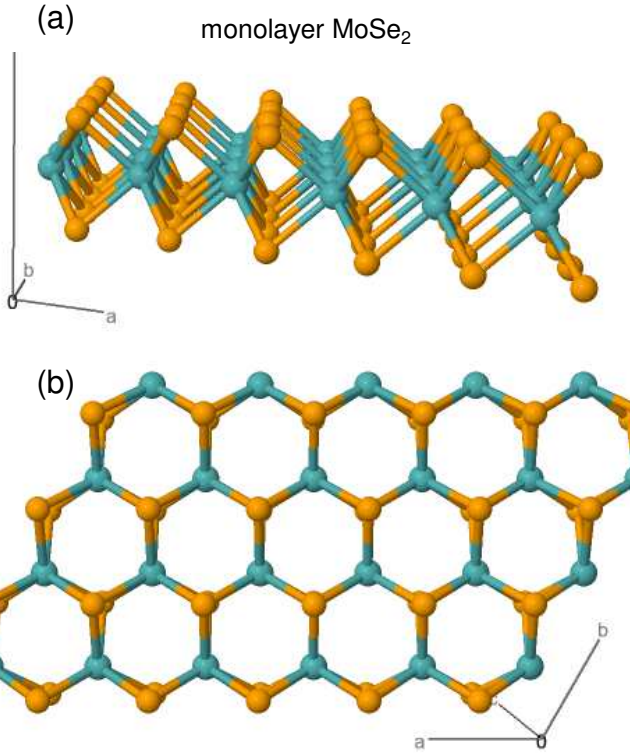

FIG. S1. Ball-and-stick model of monolayer $MoSe_2$. (a) Side and (b) top views of the monolayer. These drawings are made using the *Jmol* applet (http://www.cryst.ehu.es).

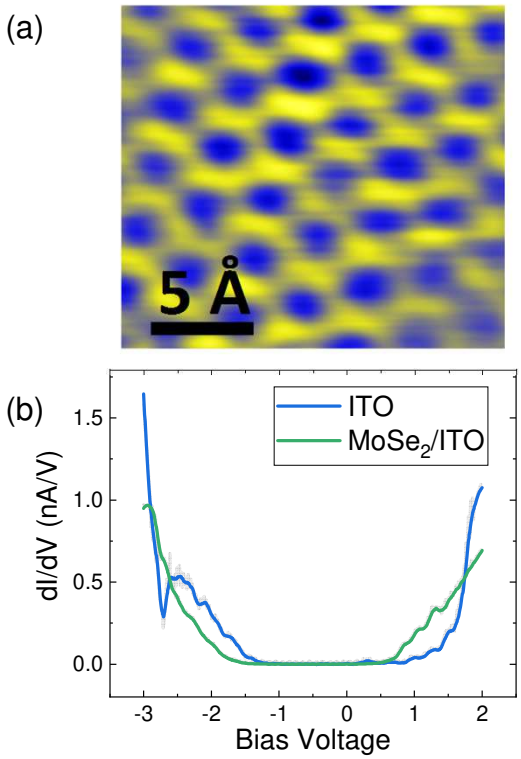

FIG. S2. (a) Atomic-resolution STM image measured on monolayer $MoSe_2$ on ITO at 300 K in ultrahigh vacuum at a sample bias of V_s = 2.4 V and a current setpoint of 10 pA. (b) dI/dV spectroscopy measurements on bare ITO (setpoint: V_s = 2.0 V, I_t = 100 pA) and on monolayer $MoSe_2$ on ITO (setpoint: V_s = 2.2 V, I_t = 400 pA), recorded under ultrahigh vacuum at 4 K.

Figure S1 shows a ball-and-stick model of monolayer $MoSe_2$. Blue and orange balls represent molybdenum and selenium atoms, respectively. A side and top view of the monolayer are shown in Figs. S1(a) and S1(b), respectively. Figure S2 shows an atomic-resolution STM image of $MoSe_2$ and dI/dV spectroscopy measurements recorded on ITO and monolayer $MoSe_2$ in ultrahigh vacuum, using a different STM than the one used in the article.

dI/dV spectroscopy of bare ITO (at low temperature) indicates that the Fermi level is nearly centered in the bandgap of ITO, in agreement with previous STM studies [S1]. Nevertheless, we observe that, at room temperature, in air and within the investigated tunneling current range (0.1 – 10 nA), STM measurements may be carried out on ITO only at positive sample bias otherwise apparent damage of the ITO occurs. Such asymmetric behavior of ITO has been reported in previous studies [S2, S3] and ascribed to surface-charge induced modifications of the electron mobility [S3]. In addition, electrochemical reactions may occur in air at negative sample bias (oxide reduction of ITO). Therefore, all results shown in the article are obtained using positive sample bias.

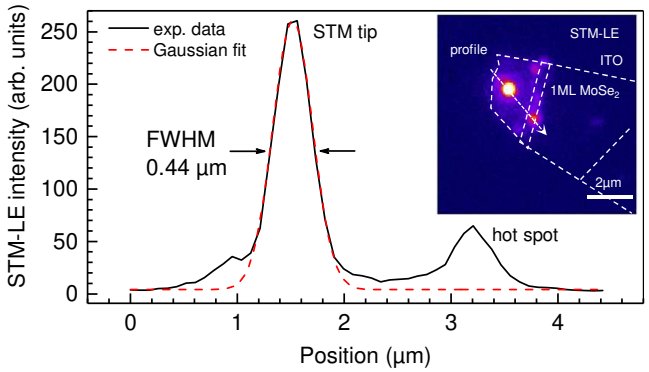

FIG. S3. Intensity profile taken along the dashed line in the real-space optical microscopy image of the STM-induced light (STM-LE) from monolayer $MoSe_2$ shown in the inset. The experimental data are fit with a Gaussian curve of full width at half maximum (FWHM) 0.44 μm. STM parameters: V_s = 4 V, I_t = 5 nA. Acquisition time: 200 s.

Intensity profile from a real-space optical image

Figure S3 shows in more detail the intensity profile shown in the inset of Fig. 3(d) in the article. The STM tip locally excites a monolayer $MoSe_2$ domain and the spatial distribution of the resulting light is measured in real space using the optical microscope. The real-space image is shown again in the inset of Fig. S3. The intensity profile is taken along a line crossing the location of the STM tip. The main peak is fit with a Gaussian curve of full width at half maximum (FWHM) 0.44 μm.

Compared PL spectra of ITO and $MoSe_2$

Figure S4 shows laser-induced photoluminescence (PL) and STM-LE spectra measured on bare ITO and on monolayer $MoSe_2$. The data measured on monolayer $MoSe_2$ [see Fig. S4(a)] are the same data as shown in the article [see Fig. 1(e)]. A semilog plot of these data is shown in Fig. S4(b), revealing more clearly the contribution from the B exciton. PL is also detected on bare ITO, the relative intensity of which is three orders of magnitude lower than that from monolayer $MoSe_2$. PL from ITO may be easily distinguished from that of $MoSe_2$ because its spectrum is comparatively broad and consists of two peaks at 1.80 eV (λ = 690 nm) and 2.30 eV (λ = 540 nm), the full widths of which are about 0.5 eV at half maximum. The STM-LE spectrum of bare ITO shown in Fig. S4(c) strongly differs from both the STM-LE of monolayer $MoSe_2$ and the PL of bare ITO, but agrees well with the expected optical scattering response of a sharp tungsten tip [S4].

Fourier-space images

Figure 2 in the article shows a Fourier-space image. This represents the angular distribution of the STM-LE from monolayer $MoSe_2$, juxtaposed with the theoretical emission patterns of an oscillating point-like electric dipole on an air-glass interface. This dipole may be oriented out-of-plane or randomly in the xy plane (i.e., the plane orthogonal to the tip axis and to the optical axis of the microscope objective). Below, we explain why a dipole randomly oriented in the xy plane (and not oriented in a single direction in the xy plane) is considered and why using only symmetry considerations we cannot determine the orientation of the transition dipole moment from the experimental Fourier-space images. To support this discussion, we show in Figure S5 the theoretical emission patterns of an oscillating point-like electric dipole on an air-glass interface, oriented (a) along the x-axis, (b) along the y-axis, and (c) randomly oriented in the xy plane.

In our study, the luminescent sample exhibits no optical anisotropy in the plane. We assume that there is no preferential in-plane orientation for the transition dipole moment of the bright excitons in monolayer $MoSe_2$. In addition, the excitation source (i.e., the tunnel current between the tip and the sample) has cylindrical symmetry with respect to the tunnel junction axis; therefore, the excitation is isotropic in the plane. Thus, the measured luminescence images are averaged over all possible in-plane orientations of the transition dipole moment of the bright excitons. As a result, the measured Fourier-space images exhibit circular symmetry with respect to the center of Fourier space. Therefore, unlike in previous work where single molecules with fixed in-plane orientation were considered [S5], the symmetry argument cannot be used in our case to distinguish between in-plane and out-of-plane emitting dipoles. In our case, emission patterns averaged over all possible in-plane orientations must be considered. Nevertheless, other arguments may be used to distinguish between in-plane and out-of-plane emitting dipoles. In particular, the subcritical angular distribution is clearly different and the angle of maximum intensity is also not the same.

Mapping

Figures 3(a) and 3(b) in the article show the STM topography and photon emission quantum efficiency maps of an area where both bilayer and monolayer $MoSe_2$ may be seen. It is noteworthy that the combined information from Figs. 3(a) and 3(b) is necessary to unambiguously identify the bilayer and monolayer areas. The two areas differ by 0.9 nm in STM height, i.e., close to the expected thickness of one $MoSe_2$ layer (0.65 nm); however, their STM heights with respect to bare ITO (i.e.,

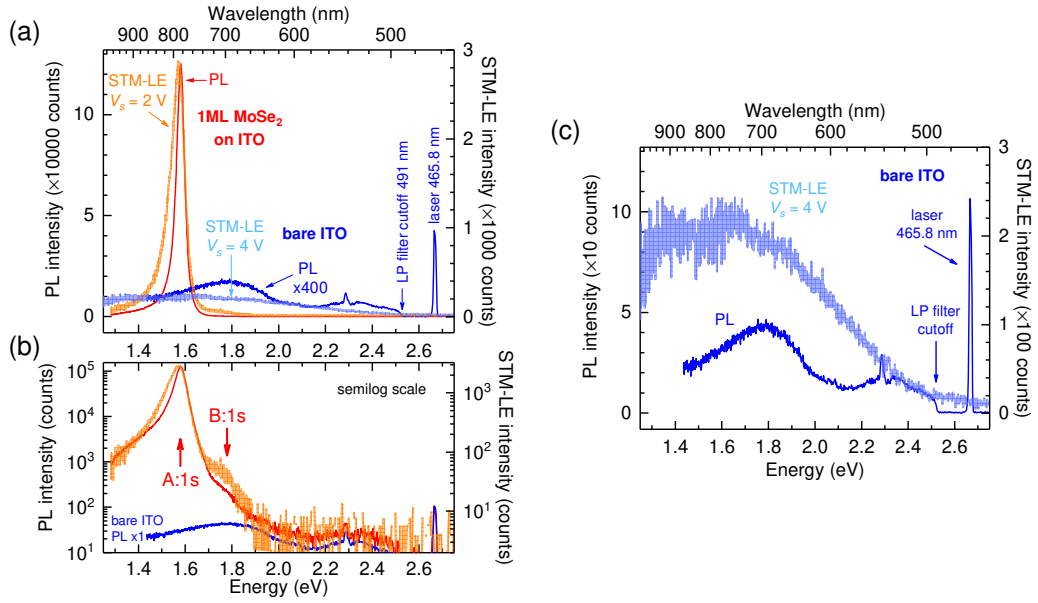

FIG. S4. Laser-induced photoluminescence (PL) and STM-induced luminescence (STM-LE) spectra of monolayer $MoSe_2$ and bare ITO. The laser is emitting at a wavelength of 465.8 nm and a longpass filter from a wavelength of 491 nm is used at detection. The STM current setpoint is 10 nA on $MoSe_2$ and 0.1 nA on ITO. Sample bias is 2 V on $MoSe_2$ and 4 V on ITO. Acquisition time is 150 s. All spectra are corrected for the detection efficiency of the apparatus (objective transmission, diffraction grating efficiency, and CCD quantum efficiency). In (b), a semilog plot of the same data shows more clearly the A:1s and B:1s exciton contributions. In (c), the PL and STM-LE data measured on ITO are presented.

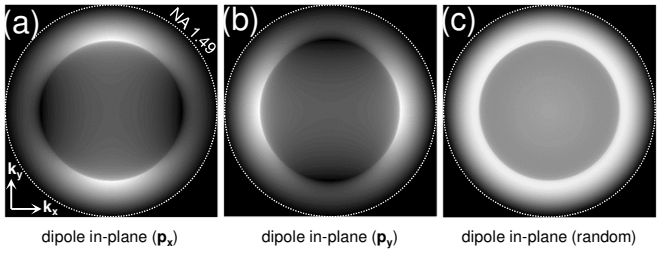

FIG. S5. Theoretical emission patterns in Fourier-space, calculated for an oscillating point-like electric dipole on an air-glass interface, oriented (a) along the x-axis, (b) along the y-axis, and (c) randomly in the xy plane.

2.7 ± 0.3 nm for the monolayer) are artificially high, primarily due to the roughness (i.e., 2.3 nm rms) of the underlying ITO surface. The photon emission quantum efficiencies measured on the two areas differ from each other by two orders of magnitude. Thus, monolayer versus bilayer $MoSe_2$ may be identified without ambiguity.

The detection efficiency

In the article, we report a photon emission quantum efficiency up to 10^{-7} photons per electron. Below, we explain how the detection efficiency of the setup is estimated. We define the detection efficiency as the product of the transmission coefficient of the microscope objective, the quantum efficiency of the detector and the diffraction efficiency of the grating in the spectrometer. These technical specifications are obtained from the providers. This yields, at the luminescence peak of monolayer $MoSe_2$ (λ_0 = 784 nm), detection efficiencies of 46% and 31% for photon mapping and optical spectrum measurements, respectively. Note that all spectra shown in Fig. 1 are corrected for the detection efficiency of the apparatus, whereas the photon counts obtained from photon maps in Fig. 3 and those retrieved from optical spectra in Fig. 4 in the article are not corrected for the detection efficiency.

In addition, there must be light emitted from the front side of the sample as well, which is not collected by the microscope objective. This is not taken into account in the detection efficiency. Thus, a photon emission quantum efficiency up to 10^{-7} photons per electron actually means, in our work, that up to 10^{-7} photons per electron are emitted in the collection cone of the microscope objective. In order to evaluate the collection efficiency of the objective, we have carried out numerical simulations of the emission pattern for an oscillating electric dipole on an ITO layer on glass. We used an analytical model [S6], where we ignored the effect of the TMD layer. The permittivity of ITO is taken from our ellipsometry measurements, i.e., $\epsilon_r = 2.2967 + 0.0756i$ at 800 nm. If the dipole is oriented parallel to the surface, we obtain that 12.4% of the radiated power is emitted above the surface, 61.1% in the substrate (among which 40.6% at supercrit-

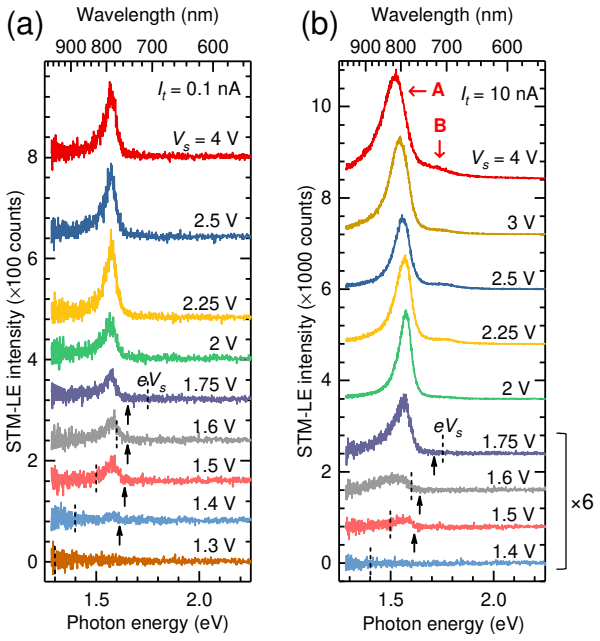

FIG. S6. STM-induced luminescence spectra of monolayer $MoSe_2$ versus sample bias at current setpoints of (a) 0.1 nA and (b) 10 nA. Arrows and dashed lines indicate the maximum emitted photon energy and the expected quantum cutoff eV_s, respectively. Acquisition time is 150 s. All spectra are corrected for the detection efficiency of the apparatus. The spectra are vertically offset for clarity.

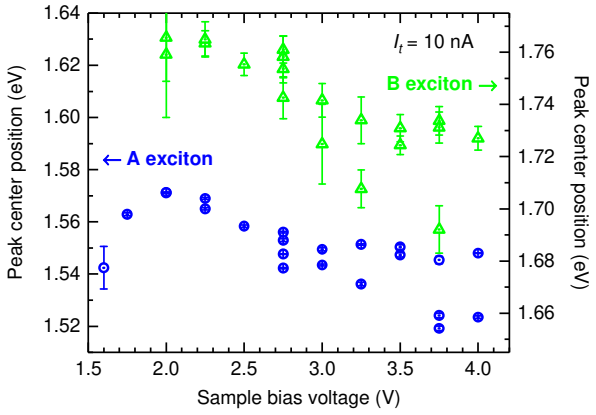

FIG. S7. Analysis of STM-induced luminescence spectra of monolayer $MoSe_2$ on ITO. Sample-bias dependence of the A and B exciton energy at a current setpoint I_t = 10 nA. Exciton energy and uncertainties (error bars) are obtained from the fit of the emission peaks with Voigt profiles.

ical angles) and 26.5% is lost or guided in the ITO layer. If the dipole is oriented orthogonally to the surface, we obtain that 10.2% of the radiated power is emitted above the surface, 59.1% in the substrate (among which 47.0% at supercritical angles) and 30.6% is lost or guided in the ITO layer. If one makes the approximation that the objective has an ideal angular aperture of 90° (NA = 1.518), instead of its actual limited aperture of 79° (NA = 1.49), then one obtains that more than 73% of the light emitted in free space is collected (one obtains 85% for a dipole orthogonal to the surface). Thus, neglecting the light emitted on the front side yields an underestimation of the total photon emission quantum efficiency by about 20 to 40%.

Bias and current dependence of the STM-LE spectra

Figures S6(a) and S6(b) show a series of spectra measured from monolayer $MoSe_2$ at current setpoints of 0.1 nA and 10 nA, respectively, and sample biases V_s varying within the 1.3-4.0 V range. The STM-LE spectra are recorded while scanning the tip on a 500×50 nm^2 area on monolayer $MoSe_2$ for averaging. The photon emission quantum efficiency plotted versus V_s in Fig. 4 of the article is obtained by dividing the area beneath the emission peaks by the integrated measured current.

The STM-LE peak position and lineshape are nearly independent of V_s at a current setpoint of 0.1 nA. The emission peak remains at 1.572±0.005 eV in energy and at about 55 meV in FWHM within the 1.5–3.0 V bias range. Stronger spectral dependence on V_s is found at a current setpoint of 10 nA compared to 0.1 nA [see Fig. S6(b)]. The emission peaks increasingly broaden and redshift as the sample bias is raised from 2 to 4 V. A quantitative analysis of the red-shift versus V_s is shown in Fig. S7.

A general tendency is observed in Fig. S7, where both the A and B exciton energies redshift by roughly 30 meV V^{-1} as the sample bias is increased within the 2–4 V range. Nevertheless, the data recorded at each bias voltage exhibit a statistical variation, with a standard deviation that increases at higher sample bias. This bias-dependent distribution is observed because each spectrum is measured on a "fresh" area of the sample, where no STM-induced luminescence experiments have been carried out before. Our motivation for proceeding in this way is to prevent any effect from possible non-reversible modifications of the luminescent sample by the STM tip. The scanned areas on the sample may exhibit slight geometrical differences, e.g., in roughness or in density of defects. In addition, different areas on the sample may exhibit slightly different coupling to the underlying ITO layer, which exhibits some spatial heterogeneity in surface conductivity on the sub micrometer scale, due to its granular geometry. Consequently, the effect of the strong electric field in the tip-substrate junction on the energy positions of the excitons may differ from an area to another. Such variations are inherent of the experimental method used, where the experiments are carried out in air on samples that are not controlled at the atomic scale; nonetheless, it is expected that such variations would not

occur if similar experiments were carried out in surface science conditions, in vacuum on an atomically flat surface.

The increasing spectral broadening and the red shift of the emission peaks when the sample bias is raised from 2 V to 4 V may be explained in several ways. First, exciton-exciton annihilation and exciton interactions with charge carriers may yield such spectral modifications of the emission peaks. Due to the low current (0.1 – 10 nA) and the low efficiency of the electrical excitation process, exciton and charge carrier densities are expected to be much lower than in previous photoluminescence and electroluminescence studies. Nevertheless, since the excitation is comparatively much more localized in our case, exciton-exciton annihilation and exciton interactions with charge carriers cannot be excluded. Secondly, the observed spectral broadening and red shift of the emission peaks may result from the Stark effect due to the strong electric field in the tip-substrate junction. However, the contribution of the Stark effect is difficult to model or to distinguish from other effects in the present case, because all STM experiments are carried out in constant current mode (not constant height) and the spatial distribution of the in-plane and out-of-plane components of the electric field in and around the tip-substrate junction may be highly heterogeneous. Finally, the observed spectral broadening and red shift of the emission peaks may also result from local heating effects, due to the electronic current.

Overbias emission

Overbias ($h\nu > eV_s$) emission is visible in Fig. S6 at low sample bias ($V_s \leq 1.6$ V), both at 0.1 nA and 10 nA. Light is emitted up to 200 meV above the quantum cutoff (eV_s) at $V_s = 1.4$ V. The high-energy tail of the emission peak exceeds the quantum cutoff in energy by an amount that apparently decreases when increasing the sample bias. This is similar to previous STM-LE studies [S7]. Nonlinear electronic processes involving surface plasmons [S8–S10] cannot be invoked here, since the tip and the substrate are made of non-plasmonic materials. Instead, overbias emission may be due to phonon-assisted upconversion processes in the TMD [S11, S12], exciton-exciton Auger scattering [S13, S14], or local heating effects under the STM tip. In general, overbias emission in electroluminescence relies on excitation mechanisms involving several electrons. Nevertheless, the data shown in Figure 4 in the article, which have been measured at setpoint currents of 0.1 nA and 10 nA, may not be used to confirm a nonlinear dependence of the overbias emission on the current. Additional experiments on the current dependence of the overbias emission are necessary to address this specific issue [S15].

Excitation mechanism

Below, we consider two excitation mechanisms that may be involved in STM-LE from a direct-bandgap semiconductor. One mechanism relies on electrical charge carrier injection as in a light emitting diode. In order to create an electron-hole pair, an electron is injected in the conduction band and, simultaneously, an electron vacancy is created in the valence band of the semiconductor. For this process to occur, electrons must be allowed to tunnel from the negatively biased electrode to the conduction band and from the valence band to the positively biased electrode. This requires an energy level arrangement that only occurs above a certain bias voltage. Such a bias voltage is generally higher (in corresponding electron energy) than the electronic band gap energy of the semiconductor [S16]. In contrast, a second mechanism is possible, which is based on resonance energy transfer, i.e., a coupling mediated by virtual photons [S17]. In a classical picture, the tunnel current generates an oscillating electric dipole in the tip-surface gap, which transfers energy to the semiconductor via near-field electromagnetic coupling. The only requirement for this process to occur is that the electron energy exceeds the optical gap energy, which differs from the "free-particle" electronic gap by the exciton binding energy. In particular, monolayer $MoSe_2$ has an optical gap of 1.58 eV and an exciton binding energy of 0.55 eV [S18–S20]. Therefore, the two possible mechanisms may be distinguished by investigating the bias dependence of the photon emission quantum efficiency and determining the lowest bias at which luminescence from $MoSe_2$ may be detected.

As shown in Fig. 4 of the article, STM-induced luminescence begins at a bias voltage between 1.4 V and 1.5 V, which matches more closely the optical gap (1.58 eV) than the free-particle electronic gap (2.13 eV). Thus, we infer that the excitation mechanism is resonance energy transfer. Nevertheless, at sufficiently high electron energies eV_s above the electronic bandgap, additional excitation mechanisms such as the diode-like mechanism described above may come into play, provided that the necessary energy level arrangement occurs.

Finally, we observe a slight difference, of about 0.1 to 0.2 eV, between the luminescence onset with increasing bias and the optical bandgap energy. This difference is consistent with the observation of overbias emission in the spectra, where light is emitted up to 0.2 eV above the quantum cut-off (eV_s) at $V_s = 1.4$ V.

Dipole orientation

Here, we clarify the apparent contradiction that STM-induced luminescence from monolayer $MoSe_2$ on ITO is primarily due to excitons that have in-plane oriented transition dipole moments, even though the tunneling

current is oriented along the direction orthogonal to the sample plane.

Most often, the emission of light from below the tip of an STM is ascribed to inelastic electric tunneling through the tip-sample junction [S21–S23]. Within a classical description, such a process is equivalent to an oscillating electric dipole, the orientation of which is orthogonal to the surface of the sample [S24]. It is generally admitted that the origin of this effect is the time-dependent fluctuations of the electronic current (i.e., the shot noise) at optical frequencies [S9, S10]. In the case of a metal surface, taking into account image charges is crucial and primarily out-of-plane optical modes are excited, due to strong enhancement of the optical fields along the tip-sample axis. However, in our case, the luminescent sample is not on a metal surface. The substrate is transparent and not metallic. Moreover, the tip is not plasmonic within the investigated frequency range. As a result, the contribution of image charges is comparatively weak. Nevertheless, due to the symmetry of the tip-surface junction, inelastic electron tunneling is expected to be equivalent to an electric dipole oscillating along the tip direction, i.e., *orthogonal* to the surface. However, this does not necessarily prevent the tunneling current from exciting excitons having their transition dipole moment *parallel* to the surface.

In the resonance energy transfer theory, the Ideal Dipole Approximation (IDA) applies when the two coupled systems are small compared to their separation distance. Within this approximation, the coupling between two orthogonal electric dipoles is indeed not efficient. However, the IDA is known to perform poorly, e.g., for finite-sized organic molecules at separation distances below 5 nm [S25]. Furthermore, the most recent literature on STM-induced luminescence of single molecules is on flat lying molecules that have in-plane transition dipole moment (see, e.g., Ref [S16]). In addition, at the nanometer scale, the STM tunnel junction cannot be described as a point-like oscillating dipole. The 2D geometry of the luminescent sample also makes the IDA inapplicable. Finally, the observation of luminescence from the bright excitons in $MoSe_2$, which have in-plane transition dipole moment, does not necessarily mean that a resonance energy transfer only occurs from the tunnel current to these bright excitons. A resonance energy transfer may also occur from the tunnel current to the dark excitons in $MoSe_2$, which have out-of-plane transition dipole moment and lie a few tens of meV above their bright counterparts. The dark excitons are expected to convert into the lower-energy bright excitons (through phonon coupling) before decaying radiatively.

Plasmon-less excitation: advantages

In this work, the absence of surface plasmons is crucial for two reasons. First, the absence of surface plasmons means that the "native" properties of the emitter, and not the properties of the emitter coupled to a plasmonic tip, a plasmonic surface, or a tip-surface plasmonic cavity, may be probed. This is key in the present study, since the previous STM-induced luminescence studies on 2D semiconductors have not shown native excitonic properties; instead, only plasmonic emission was observed, which does not reveal the excitonic properties of the 2D semiconductors [S26]. Moreover, the presence of a localized surface plasmon in the tip-surface gap is expected to strongly modify the emission processes by enhancing (by orders of magnitude) the radiative rate of the out-of-plane modes of the emitter, as compared to the in-plane modes [S27]. As a result, the emission may be dominated by (otherwise dark) excitons that have an out-of-plane transition dipole moment, to the expense of (otherwise bright) excitons that have an in-plane transition dipole moment [S28, S29]. Secondly, the mechanisms previously considered to explain STM-induced luminescence from semiconducting nanostructures and organic molecules involve the excitation of localized surface plasmons in the tip-surface gap, which makes it difficult to identify the elementary excitation processes [S30]. Our work shows that an energy transfer from the tunnel current to the emitter may occur directly, through virtual photons, without any coupling to a plasmonic mode.

* eric.le-moal@u-psud.fr

[S1] F. Matino, L. Persano, V. Arima, D. Pisignano, R. I. R. Blyth, R. Cingolani, and R. Rinaldi, Phys. Rev. B **72**, 085437 (2005).

[S2] S. Dasgupta, M. Lukas, K. Dössel, R. Kruk, and H. Hahn, Phys. Rev. B **80**, 085425 (2009).

[S3] P. D. C. King, T. D. Veal, F. Fuchs, C. Y. Wang, D. J. Payne, A. Bourlange, H. Zhang, G. R. Bell, V. Cimalla, O. Ambacher, R. G. Egdell, F. Bechstedt, and C. F. McConville, Phys. Rev. B **79**, 205211 (2009).

[S4] C. C. Neacsu, G. A. Steudle, and M. B. Raschke, Appl. Phys. B **80**, 295 (2005).

[S5] M. A. Lieb, J. M. Zavislan, and L. Novotny, J. Opt. Soc. Am. B **21**, 1210 (2004).

[S6] L. Novotny and B. Hecht, *Principles of Nano-Optics* (Cambridge University Press, 2006) DOI: 10.1017/CBO9780511813535.

[S7] R. Pechou, R. Coratger, F. Ajustron, and J. Beauvillain, Appl. Phys. Lett. **72**, 671 (1998).

[S8] G. Schull, N. Néel, P. Johansson, and R. Berndt, Phys. Rev. Lett. **102**, 057401 (2009).

[S9] N. Schneider, P. Johansson, and R. Berndt, Phys. Rev. B **87**, 045409 (2013).

[S10] F. Xu, C. Holmqvist, and W. Belzig, Phys. Rev. Lett. **113**, 066801 (2014).

[S11] A. M. Jones, H. Yu, J. R. Schaibley, J. Yan, D. G. Mandrus, T. Taniguchi, K. Watanabe, H. Dery, W. Yao, and X. Xu, Nat. Phys. **12**, 323 (2015).
[S12] J. Jadczak, L. Bryja, J. Kutrowska-Girzycka, P. Kapuściński, M. Bieniek, Y.-S. Huang, and P. Hawrylak, Nat. Commun. **10**, 107 (2019).
[S13] M. Manca, M. M. Glazov, C. Robert, F. Cadiz, T. Taniguchi, K. Watanabe, E. Courtade, T. Amand, P. Renucci, X. Marie, G. Wang, and B. Urbaszek, Nat. Commun. **8**, 14927 (2017).
[S14] B. Han, C. Robert, E. Courtade, M. Manca, S. Shree, T. Amand, P. Renucci, T. Taniguchi, K. Watanabe, X. Marie, L. E. Golub, M. M. Glazov, and B. Urbaszek, Phys. Rev. X **8**, 031073 (2018).
[S15] G. Chen, Y. Luo, H. Gao, J. Jiang, Y. Yu, L. Zhang, Y. Zhang, X. Li, Z. Zhang, and Z. Dong, Phys. Rev. Lett. **122**, 177401 (2019).
[S16] B. Doppagne, M. C. Chong, E. Lorchat, S. Berciaud, M. Romeo, H. Bulou, A. Boeglin, F. Scheurer, and G. Schull, Phys. Rev. Lett. **118**, 127401 (2017).
[S17] D. L. Andrews and D. S. Bradshaw, Ann. Phys. **526**, 173 (2014).
[S18] M. M. Ugeda, A. J. Bradley, S.-F. Shi, F. H. da Jornada, Y. Zhang, D. Y. Qiu, W. Ruan, S.-K. Mo, Z. Hussain, Z.-X. Shen, F. Wang, S. G. Louie, and M. F. Crommie, Nat. Mater. **13**, 1091 (2014).
[S19] M. Koperski, M. R. Molas, A. Arora, K. Nogajewski, A. O. Slobodeniuk, C. Faugeras, and M. Potemski, Nanophotonics **6**, 1289 (2017).
[S20] G. Wang, A. Chernikov, M. M. Glazov, T. F. Heinz, X. Marie, T. Amand, and B. Urbaszek, Rev. Mod. Phys. **90**, 021001 (2018).
[S21] J. Lambe and S. L. McCarthy, Phys. Rev. Lett. **37**, 923 (1976).
[S22] J. K. Gimzewski, J. K. Sass, R. R. Schlitter, and J. Schott, Europhys. Lett. **8**, 435 (1989).
[S23] R. Berndt, J. K. Gimzewski, and P. Johansson, Phys. Rev. Lett. **67**, 3796 (1991).
[S24] P. Johansson, Phys. Rev. B **58**, 10823 (1998).
[S25] A. Muñoz Losa, C. Curutchet, B. P. Krueger, L. R. Hartsell, and B. Mennucci, Biophys. J. **96**, 4779 (2009).
[S26] N. Krane, C. Lotze, J. M. Läger, G. Reecht, and K. J. Franke, Nano Lett. **16**, 5163 (2016).
[S27] E. Le Moal, S. Marguet, D. Canneson, B. Rogez, E. Boer-Duchemin, G. Dujardin, T. V. Teperik, D.-C. Marinica, and A. G. Borisov, Phys. Rev. B **93**, 035418 (2016).
[S28] K.-D. Park, O. Khatib, V. Kravtsov, G. Clark, X. Xu, and M. B. Raschke, Nano Lett. **16**, 2621 (2016).
[S29] K.-D. Park, T. Jiang, G. Clark, X. Xu, and M. B. Raschke, Nat. Nanotechnol. **13**, 59 (2018).
[S30] Z. C. Dong, X. L. Zhang, H. Y. Gao, Y. Luo, C. Zhang, L. G. Chen, R. Zhang, X. Tao, Y. Zhang, J. L. Yang, and J. G. Hou, Nat. Photonics **4**, 50 (2009).